The Effect of Drag Model on Heatshield Recession due to Particle Impacts for Martian Spacecraft

Grant Palmer[1] and Amal Sahai[2]
AMA, Inc. at NASA Ames Research Center, Moffett Field, CA, 94035, United States

A spacecraft entering the Martian atmosphere during a dust storm may experience recession to the heatshield due to dust particle impacts. Aerodynamic drag is the primary force that determines the trajectory of the dust particles through the shock layer. This paper examines the effect of particle drag model on the heatshield recession. Three particle drag models are assessed including two that are intended to be applicable over a wide range of particle flow conditions. Particle trajectories are computed in conditions measured during the 2007 major global dust storm. It was found that accounting for Knudsen number and compressibility effects made a large difference in the estimated particle impact velocity. The two drag models that were valid for transitional, compressible particle flow environments predicted only slightly-different amounts of heatshield recession due to dust particle impacts. A brief description of the effects of non-spherical particles on drag coefficients is provided.

Nomenclature

A = cross-sectional area, m^2
c = speed of sound, m/s
C_D = drag coefficient
d_p = particle diameter, m
$d_z\tau$ = dust opacity, 1/km
F_D = drag force, N
Kn = Knudsen number
m = mass, kg
M = Mach number
$n(r)$ = normalized particle size distribution, 1/m
$N(r)$ = particle size distribution, 1/m^4
N_v = volumetric number density, 1/m^3
r_m = mode radius, m
Re = Reynolds number
$\vec{v}$ = velocity, m/s
μ = viscosity, kg/m-s
ρ = density, kg/m^3

Subscripts
g = gas
p = particle

[1] Research Scientist, Aerothermodynamics Branch, AIAA Associate Fellow.
[2] Research Scientist, Aerothermodynamics Branch, AIAA member

I. Introduction

The analysis of dust-laden flows can be an important element of spacecraft design. For example, a spacecraft entering the Martian atmosphere will encounter dust particles suspended in the atmosphere. If the entry occurs during a major regional or global dust storm, dust particle impacts on the heatshield of the spacecraft can cause erosion of the vehicle thermal protection system (TPS) that can be equivalent to that caused by thermochemical ablation [1].

Developing a simulation capability to model dust-laden flows requires the ability to accurately predict the velocity of a particle as it travels through a shock layer, nozzle plume, or the flow of an experimental facility. The primary mechanism that determines the particle velocity is the drag force acting on the particle. The drag force is typically expressed in terms of the frontal area of the particle, its velocity relative to the surrounding fluid, the density of the surrounding fluid, and a non-dimensional number called the drag coefficient. A considerable amount of effort has been devoted over many decades to the development of models or correlations to estimate the drag coefficient for spherical bodies over a wide range of flow conditions [2]-[7]. The correlations have historically been based on experimental data, but more recently computational simulations have been used to augment the experimental data [2].

Most recently developed particle drag models are designed to be applicable under a wide range of particle flow conditions from free-molecular to continuum, incompressible to hypersonic, and over a wide range of particles Reynolds numbers. The Martian entry condition, however, takes place over a more limited range of particle flow conditions. The question this paper examines is whether and to what extent the choice of particle drag model affects the estimated heatshield recession due to dust particle impacts.

As part of the NASA Entry Systems Modeling (ESM) project under the NASA Game Changing Development (GCD) program, an integrated CFD-particle trajectory code named US3D-DUST is being developed [8]. This code uses a Lagrangian-based framework that computes the trajectories of individual particles in the flow. Several of the commonly used spherical drag models have been implemented in US3D-DUST including the Henderson [5] and Loth 2021 [2] models.

In this study, the US3D-DUST code will be used to simulate particle flows in the shock layer of the Schiaparelli capsule that entered the Martian atmosphere in 2016 [9]. The Schiaparelli capsule entered during quiescent dust conditions, but in order to test the different drag models, the dust environments simulated in this paper are based on conditions measured during the 2007 major global dust storm. The heatshield recession will be computed by US3D-DUST using various particle drag models to assess the effect the choice of drag model has on the surface recession.

II. Characterizing Dusty Flow Environments

The flow environment experienced by a particle traveling through a shock layer or the flow through an experimental facility can be characterized in terms of the particle Mach, Reynolds, and Knudsen numbers. These non-dimensional numbers are similar to the standard definitions applied to gas flows, with the difference being that the particle non-dimensional numbers are based on the relative particle velocity, $\Delta\vec{V}$, between the particle and the surrounding fluid.

$$\Delta\vec{V} = \overrightarrow{v_g} - \overrightarrow{v_p} \tag{1}$$

A. Reynolds Number

The particle Reynolds is the ratio of the inertial and viscous forces acting on the particle and is a function of the relative particle velocity, the particle diameter, and the density and viscosity of the fluid surrounding the particle.

$$Re = \frac{\rho_g |\Delta\vec{V}| d_p}{\mu_g} \tag{2}$$

The particle Reynolds number determines the nature of the boundary layer flow around the particle. If the particle Reynolds number is much less than 1, the particle is in a flow condition known as the "creeping flow" regime [2]. Viscous effects dominate, and the flow is laminar and fully-attached over the entire particle. This condition is also referred to as the Stokes drag regime in reference to the early experimental work performed by Stokes [4]. The boundary layer around the particle continues to be laminar and attached for particle Reynolds numbers less than 20. As Reynolds numbers continue to increase up to a value of about Re = 130, the wake flow behind the particle is separated but steady. At still higher Reynolds numbers, up to Re = 1500, the laminar wake becomes unsteady and transitional. For Reynolds numbers between 2000 and 2.0×10^5, a laminar boundary layer on the front of the sphere will separate at an angle of 80 degrees, and this flow separation creates a fully turbulent wake behind the particle [2]. The drag coefficient in this region is more or less constant with a value between 0.4 and 0.45, a value known as the "critical drag coefficient". This constant drag coefficient behavior was noticed by Newton in 1710.

The different boundary layer flow regions described in the previous paragraph for incompressible, continuum flow are shown graphically in Fig. 1, which was taken from Ref. [2]. Also shown on the curve are some of the drag coefficient correlations that will be described in Section III.

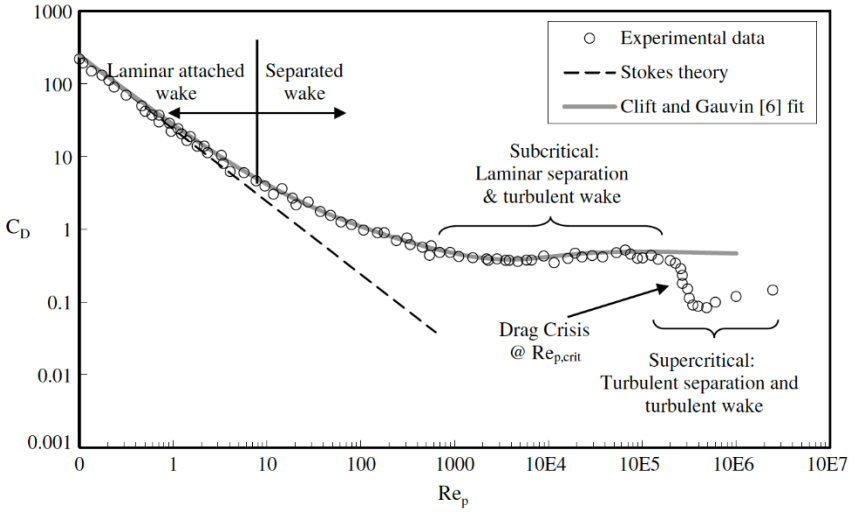


Figure 1. Drag coefficient as a function of particle Reynolds number for incompressible, continuum flow, from Ref. [2].

B. Mach Number

The particle Mach number characterizes the extent of compressibility effects on the flow around the particle and is equal to the magnitude of the relative particle velocity divided by the speed of sound in the fluid surrounding the particle.

$$M = \frac{|\Delta\vec{V}|}{c} \tag{3}$$

Because the particle Mach number is based on the relative particle velocity, a slow-moving particle striking a fast-moving shock layer (e.g., in front of a spacecraft) and a fast-moving particle striking a stationary shock wave (e.g., in front of a model in an arcjet experiment) can both experience supersonic particle Mach numbers

The different compressibility flow regimes are shown in Table 1. At low particle Mach numbers, compressibility effects are negligible, and the flow can be assumed to be incompressible. At particle Mach numbers between 0.1 and 0.65, the flow is still subsonic, but compressibility effects have increased to the point that they must be included in the drag model [3]. As the particle Mach number continues to increase, the flow regime will evolve from subsonic to transonic and eventually supersonic conditions. Hypersonic flow conditions are present for Mach numbers greater than 5. Mach number primarily affects the particle drag coefficient in the compression-dominated drag regime when the particle Reynolds number is greater than 45.

Table 1. Compressibility flow regimes.

Flow Regime	M
Incompressible	< 0.1
Compressible, subsonic	0.1 – 0.65
Transonic	0.65 – 1.2
Supersonic	1.2 – 5
Hypersonic	> 5

C. Knudsen Number

The particle Knudsen number is defined as the ratio of the mean free path of the fluid surrounding the particle to the particle diameter. The Knudsen number can be expressed in terms of the particle Mach and Reynolds numbers [2].

$$Kn = \sqrt{\frac{\pi\gamma}{2}}\left(\frac{M}{Re}\right) \tag{4}$$

The γ term in Eq. (4) is the specific heat ratio of the surrounding fluid. Since the Knudsen number is a function of the Mach and Reynolds numbers, the three quantities are not mutually independent. Specifying the values of two of them will define the third.

The four rarefaction flow regimes defined in terms of the particle Knudsen number are shown in Table 2. Continuum flow occurs when the Knudsen number is less than 0.01 and indicates that the particle Reynolds number is larger than the particle Mach number by two orders of magnitude or more. The slip regime is defined by Knudsen numbers between 0.01 and 0.1. At still higher Knudsen numbers between 0.1 and 10, the particle is in the transitional flow regime. Free molecular flow occurs when the Knudsen number is greater than 10. In the rarefaction-dominated drag regime where Re < 45, drag coefficient decreases with increasing Knudsen number, which intuitively makes sense because free-molecular conditions will offer less drag resistance than continuum flows.

Table 2. Rarefaction flow regimes

Flow Regime	Kn
Continuum	< 0.01
Slip	0.01 – 0.1
Transitional	0.1 - 10
Free-molecular	> 10

D. General Trends in Drag Coefficient

The general trends of spherical drag coefficient with regards to Reynolds, Mach, and Knudsen number are shown in Fig. 2. As presented by Loth [3], the particle Reynolds number defines two distinct regions of spherical drag coefficients. There is a "nexus" condition at Re = 45 where drag coefficient is independent of both Mach and Knudsen number with a value of approximately 1.63. At Reynolds numbers less than 45, the particles are in the rarefaction-dominated regime where Knudsen number has a strong effect on the drag coefficient. In this drag regime, the upper-bound limiting curve is the Stokes curve that represents incompressible, continuum, low Reynolds number flow. The lower-bound limiting curve in the rarefaction-dominated regime is for free-molecular flow where the drag coefficient has a value of around 2 at low Reynolds numbers and decreases slightly as Reynolds number increases.

At Reynolds numbers larger than 45, the particles are in the compression-dominated drag regime where the drag coefficient is primarily influenced by compressibility (i.e., Mach number) effects. The lower-bound curve in the compression-dominated regime is for incompressible, low Mach number flow where the drag coefficient value reaches the "critical drag coefficient" value of 0.42 – 0.45. The upper-bound limiting curve is for Mach >> 1.

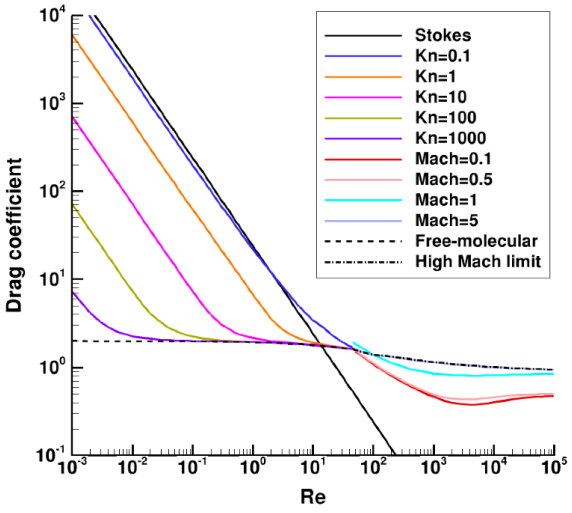


Figure 2. General trends of particle drag coefficient.

III. Particle Drag Correlations

The Lagrangian approach to determine the particle velocity as it travels through the shock layer was discussed by Bailey and Hiatt [11] and used by Papadopoulos, et al. [12] in the development of their dust erosion model. The change in location, velocity, temperature, and size of an individual particle is

determined by solving a set of coupled ordinary differential equations. The primary force acting on a particle traveling through a fluid is the aerodynamic drag force, $\overrightarrow{F_D}$, exerted on the particle. The quasi-steady drag force is assumed to be a function of the density of the surrounding fluid, the relative velocity of the particle, the frontal area of the particle, and a non-dimensional drag coefficient, C_D.

$$\overrightarrow{F_D} = \frac{1}{2}\rho_g \left|\Delta \vec{V}\right| \Delta \vec{V} C_D A \tag{5}$$

The term "quasi-steady" is used because as particle Reynolds number increases and the wake flow becomes separated and unsteady, the drag will oscillate. The quasi-steady drag force expressed in Eq. (5) represents the time-average value. Aerodynamic drag force acts along the relative velocity vector of the particle, $\overrightarrow{V_p}$. The change in velocity of the particle can be determined by applying Newton's second law of motion where the force acting on the particle is due to the aerodynamic drag on the particle.

$$m_p \frac{d\overrightarrow{V_p}}{dt} = \frac{1}{2}\rho_g \left|\Delta \vec{V}\right| \Delta \vec{V} C_D A \tag{6}$$

If the particles are assumed to be spherical and of uniform composition, the mass of the particle and frontal area can be related to the particle diameter. The change in the relative velocity for a spherical particle is a function of the density of the particle material and surrounding fluid, the particle diameter, the relative particle velocity, and the drag coefficient.

$$\frac{d\overrightarrow{V_p}}{dt} = \frac{3}{4}\frac{\rho_g}{\rho_p}\frac{C_D}{d_p} \cdot \left|\Delta \vec{V}\right| \Delta \vec{V} \tag{9}$$

Most of the theoretical and numerical simulations of particle trajectories assume spherical particles. There are two reasons for this assumption. The first reason, as previously stated, is that it allows simple relations between the particle mass and frontal area and the particle diameter. The second reason is that much of the historical experiments on which the drag models were calibrated involved firing or dropping spherical objects and measuring their velocity as they traveled through the surrounding fluid.

Of the components that make up Eq. (9), the density of the particle material and surrounding fluid, the particle diameter, and the velocity of the surrounding fluid are either known quantities or ones that are relatively straightforward to compute. The key to accurately simulating particle trajectories is therefore an accurate estimate of the drag coefficient of the particle.

A. Early drag coefficient models for incompressible, continuum flow

Early spherical drag correlations were based on experiments that were possible at the time such as measuring the velocity of a sphere dropped from a height. One of the earliest drag correlations for spherical particles was developed by Stokes [4] for incompressible continuum flows with $Re \ll 1$. According to the Stokes derivation, the drag coefficient of the sphere is linear with the inverse of particle Reynolds number.

$$C_D = \frac{24}{Re} \tag{6}$$

Looking at Fig. 1, the experimental data indicates a linear drag coefficient behavior at low Reynolds numbers. As Reynolds number increases, the spherical drag coefficient deviates from, and is higher than,

the linear value predicted by the Stokes correlation. For Reynolds numbers between 0.1 and 10, the flow behind the particle transitions from an attached laminar wake to a separated but still laminar wake. As Reynolds numbers continue to increase up to values of about 2000, the wake behind the particle becomes unsteady and transitional. As shown in Fig. 1, these changes to the wake flow cause the drag force and drag coefficient to increasingly deviate above the linear Stokes correlation value.

As presented by Loth, et al. [2], the general expression for a particle drag coefficient for incompressible continuum flow at finite values of Reynolds number can be expressed as the Stokes correlation drag coefficient value multiplied by a Stokes correction factor, f, that accounts for Reynolds number effects.

$$C_D = \frac{24}{Re} f \tag{7}$$

To extend the Stokes correlation for higher Reynolds numbers, Clift and Gauvin [6] developed a correlation that multiplies the Stokes equation by a Stokes correction factor term, and the correlation also adds a second term that transitions to the critical drag coefficient value of 0.42 at Reynolds numbers above 2000.

$$C_D = \frac{24}{Re}(1 + 0.15Re^{0.687}) + \frac{0.42}{1+(42500/Re^{1.16})} \tag{8}$$

The left-hand term of Eq. (8), consisting of the Stokes correlation and correction factor is known as the Schiller-Naumann drag correlation [8] and can be used by itself for particle Reynolds numbers less than 800.

B. The Henderson drag model

The Stokes and Clift-Gauvin drag correlations are intended for spherical particles traveling through incompressible continuum flows. A more ambitious drag model for spheres was developed by Henderson [5] that is designed to be applicable to all flow regimes. Until recently, the Henderson model was commonly used and considered to be the most accurate drag model for high-speed particle trajectory analysis. The Henderson drag model provides two equations that are applicable for subsonic and supersonic flows in continuum, slip, transitional, and free-molecular flow regimes.

The Henderson model equations are primarily designed to match the experimental data of Bailey and Hiatt [11] that fired spheres made from various materials ranging in size from 2.38 – 25.4 mm in a ballistic range at Mach numbers ranging from 0.13 to 7. The particle Reynolds numbers in the test shots varied from 4.9 – 77.4x10^3. The drag coefficient was inferred from the velocity decrease of the spheres during the test. In Ref. [3] it is mentioned that there were difficulties during the experiments reported by Bailey and Hiatt in measuring the drag coefficient in the transonic Mach regime, specifically for lower particle Reynolds numbers. It is stated that for 20 < Re < 200, the change from subsonic to supersonic drag values is accompanied by relatively large changes in drag coefficient for small changes in Mach. In addition to the Bailey and Hiatt data, the Henderson correlations are also based on earlier theoretical derivations and experimental data by Milikan [13], [14]

The Henderson correlations are constructed such that they reduce to the incompressible, subsonic and free-molecular limits for the corresponding values of Reynolds, Mach, and Knudsen numbers. The correlations are intended for particle Mach numbers up to 6 and Reynolds numbers up to the laminar-turbulent transition, which Loth [2] estimated occurs at Reynolds numbers of around 1500. The

Henderson model accounts for temperature differences between the surface of the particle and the surrounding fluid.

The Henderson drag coefficient equation for subsonic flow is a function of the particle Mach, Reynolds, and Knudsen numbers and the particle and fluid temperatures.

$$C_D = 24\left[Re + S\left\{4.33 + \left(\frac{3.65-1.53\frac{T_p}{T_g}}{1+0.353\frac{T_p}{T_g}}\right)exp\left(-0.247\frac{Re}{S}\right)\right\}\right]^{-1} + exp\left(-0.5\frac{M}{\sqrt{Re}}\right)\left[\frac{4.5+0.38\left(0.03Re+0.48\sqrt{Re}\right)}{1+0.03Re+0.48\sqrt{Re}} + 0.1M^2 + 0.2M^8\right] + 0.6S\left[1 - exp\left(-\frac{M}{Re}\right)\right] \quad (9)$$

The molecular speed ratio, S, is a function of particle Mach number, M, and is defined as:

$$S = M\sqrt{\frac{\gamma}{2}} \quad (10)$$

The subsonic equation for drag coefficient shown in Eq. (9) is complicated in part because it is designed to bridge and be applicable for the various particle flow regimes. At conditions of low Knudsen number and high Reynolds number (i.e., continuum flow), the equation reduces to the Stokes-Oseen equation, $C_d = 24Re^{-1} + 4.5$. If the particle Reynolds number approaches zero, the subsonic equation simplifies to the theoretical expression for free molecular flow. The exponential factors in the second and third terms of Eq. (9) were derived to agree with the Bailey and Hiatt experimental data.

For supersonic Mach numbers greater than 1.75, the Henderson model uses the following expression:

$$C_D = 0.9 + \frac{0.34}{M^2} + 1.86\sqrt{\frac{M}{Re}}\left[2 + \frac{2}{S^2} + \frac{1.058}{S}\sqrt{\frac{T_p}{T_g}} - \frac{1}{S^4}\right]\Big/\left(1 + 1.86\sqrt{\frac{M}{Re}}\right) \quad (11)$$

The supersonic equation is also designed to cover the various flow regimes. For free molecular flow where the Reynolds number approaches zero, the equation reduces to the terms inside the square brackets. For low Knudsen number, high Reynolds number continuum flow, the equation simplifies to the first two terms in the numerator. For supersonic slip and transitional flow, the equation is designed to give good agreement with experimental data of Bailey and Hiatt [11]

One weakness of the Henderson correlation is that there is a gap between the subsonic correlation that goes up to Mach = 1 and the supersonic correlation that starts at a Mach number of 1.75. It is not clear why this gap exists, since there is experimental data from Bailey and Hiatt at Mach numbers between 1 and 1.75, but it is stated in Ref. [11] that there were large changes in drag coefficient for small changes in Mach number in the transonic flow regime, so perhaps that data was suspect. Whatever the reason, for particle Mach numbers between 1.0 and 1.75, Henderson recommended a linear interpolation between the drag coefficients at Mach 1 and 1.75.

$$C_D = C_D(1.0) + \frac{4}{3}(M-1)[C_D(1.75) - C_D(1.0)] \quad (12)$$

Another deficiency of the Henderson model when it is applied to particles traveling through Martian shock layers is that the coefficients and general form of the equations are meant to match the experimental data of Bailey and Hiatt, but almost all of that data is in the continuum and slip flow regimes. Of the 490 data points presented in Ref. [11], 373 of them are for continuum flow conditions and 108 sets of data are in the slip flow regime. There are only 9 cases that were run in transitional flow

conditions, and all of them were run at the low end of transitional Knudsen numbers with a maximum Knudsen number value of 0.138. Therefore, very little experimental data is used to anchor the Henderson model in the transitional flow regime which is the relevant condition for Martian shock layer analysis.

C. The Loth drag model

In 2008, Loth [3] presented a new spherical drag model that consisted of separate correlations for the rarefaction- and compression-dominated regimes shown in Fig. 2. In addition to the Bailey and Hiatt data, the Loth correlations were also based on additional ballistic range experimental data including that of Hoerner [15], Carlson and Hoglund [16], and Macrossan [17]. In 2021, Loth, et al. [2] updated the 2008 drag model with additional experimental data as well as DSMC simulations that were used to provide data at lower particle Reynolds numbers in the slip and transitional flow regimes. The DSMC simulations confirmed observations in more recent experiments that the assumed nexus point where all of the drag coefficient curves coalesce to a single value at Re = 45 is not a single point but rather a weak transonic bump that bridges the rarefaction- and compression-dominated regimes [2].

The Loth 2021 drag model consists of two sets of correlations - one for the rarefaction-dominated drag regime where Re < 45 and a second set of correlations for the compression-dominated drag regime when Re > 45. In the rarefaction-dominated regime there are two limiting cases for drag coefficient. The upper bound of drag coefficient values is the incompressible continuum limit for Reynolds numbers much less than one, i.e., the Stokes curve, where the Knudsen number approaches zero. For low Mach number flows with non-zero Knudsen numbers, the drag coefficient in the rarefied-dominated regime can be expressed as the Schiller-Naumann component of the Clift-Gauvin correlation multiplied by a correction factor, f_{Kn}, that accounts for Knudsen number effects [2].

$$C_{D,Kn,Re} = \frac{24}{Re}(1 + 0.15Re^{0.687})f_{Kn} \tag{13}$$

Note that the second term in the Clift-Gauvin correlation is ignored in the development of Eq. (13) because it is negligible in the rarefaction-dominated regime. For small Mach numbers, Clift and Gauvin [18] developed a relation for the correction factor that agrees with approximate theory, experimental data, and more recent DMSC computations [7].

$$f_{Kn} = \frac{1}{1+K_n\left[2.514+0.8\exp\left(-\frac{0.55}{Kn}\right)\right]} \tag{14}$$

Equations (13) and (14) are intended for low particle Mach numbers where compressibility effects are minimal. For low values of Knudsen number, the value of f_{Kn} approaches 1, and Eq. (13) reduces to the Schiller-Naumann correlation. At high values of Knudsen number (i.e., free-molecular flow) the value of the correction factor approaches zero.

The other limiting case in the rarefaction-dominated regime is for free-molecular flow, where it is assumed that the particle Mach and Knudsen numbers are high. The correlation for the free molecular drag coefficient presented in Ref. [2] is attributed to Stalder and Zuric [19] and Schaff and Chambre [20] and is a function of the molecular speed ratio defined in Eq. (10) and the error function.

$$C_{D,fm} = \frac{\left(1+2S^2\right)exp\left(-S^2\right)}{S^3\sqrt{\pi}} + \frac{\left(4S^4+4S-1\right)\mathrm{erf}\,(S)}{2S^4} + \frac{2}{3S}\sqrt{\pi} \tag{15}$$

When the molecular speed ratio, and therefore particle Mach number, become very large, the value of $C_{D,fm}$ approaches 2, which is the lower limit of drag coefficient in rarefied flow for low Reynolds numbers. For larger Reynolds numbers, the free-molecular drag coefficient is modified using an empirical scaling factor.

$$C_{D,fm,Re} = \frac{C_{D,fm}}{1+[(C_{D,fm}/J_M)-1]\sqrt{Re/45}} \tag{16}$$

$$J_M = 2.26 - \frac{0.1}{M} + \frac{0.14}{M^3} \qquad M \leq 1 \tag{17a}$$

$$J_M = 1.6 + \frac{0.25}{M} + \frac{0.11}{M^2} + \frac{0.44}{M^3} \qquad M > 1 \tag{17b}$$

To determine the overall drag coefficient in the rarefaction-dominated regime where Re < 45, the low Mach number expression from Eq. (13) is blended with the high Mach number correlation shown in Eq. (16) using the particle Mach number.

$$C_D = \frac{C_{D,Kn,Re}}{1+M^4} + \frac{M^4 C_{D,fm,Re}}{1+M^4} \tag{18}$$

In the compression-dominated drag regime when Re > 45, compressibility (i.e., Mach number) effects become important. As seen in Fig. 1, the spherical drag coefficient for incompressible, continuum flow in the compression-dominated drag regime decreases gradually before reaching the critical drag coefficient value of about 0.42 for Reynolds numbers less than 2.0×10^5. The drag coefficient for incompressible, continuum flow can be estimated using the Clift-Gauvin correlation shown in Eq. (7).

It is well-known that increasing Mach number in the compression-dominated regime will increase drag coefficient [2]. To account for Mach number effects, Loth, et al. [2] propose a modified Clift-Gauvin expression that shows a good match to the available experimental and simulation data over a Mach number range from 0.25 to 10.

$$C_D = \frac{24}{Re}(1 + 0.15Re^{0.687})H_M + \frac{0.42C_M}{1+\left({}^{42500}/_{Re^{1.16}C_M}\right)+\left({}^{G_M}/_{Re^{0.5}}\right)} \tag{19}$$

$$C_M = 1.65 + 0.65\tanh(4M - 3.4) \qquad \text{for } M < 1.5 \tag{20a}$$

$$C_M = 2.18 - 0.13\tanh(0.9M - 2.7) \qquad \text{for } M > 1.5 \tag{20b}$$

$$G_M = 166M^3 + 3.29M^2 - 10.9M + 20 \qquad \text{for } M < 0.8 \tag{21a}$$

$$G_M = 5 + 40M^{-3} \qquad \text{for } M > 0.8 \tag{21a}$$

$$H_M = 0.0239M^3 + 0.212M^2 - 0.074M + 1 \qquad \text{for } M < 1 \tag{22a}$$

$$H_M = 0.93 + \frac{1}{(3.5+M^5)} \qquad \text{for } M > 1 \tag{22a}$$

A limiting case for the Loth drag correlation in the compression-dominated regime is for high Mach numbers where $M \ll 1$. In this situation, the coefficients shown in Eqs. (20) – (21) reduce to single values.

$$C_M = 2.05 \qquad G_M = 5 \qquad H_M = 0.93 \tag{23}$$

$$C_D = \frac{22.32}{Re}(1 + 0.15Re^{0.687}) + \frac{0.861}{1+\left({}^{42500}/_{Re^{2.38}}\right)+\left({}^{5}/_{Re^{0.5}}\right)} \tag{24}$$

IV. The US3D-DUST Code

The US3D code is a Navier-Stokes flow solver that was developed at the University of Minnesota in collaboration with the NASA Ames Research Center for the simulation of compressible and reacting flows [21]. The US3D code has been applied to a wide range of aeronautical and aerothermal flow problems and is one of the main CFD codes used by the NASA Entry, Descent, and Landing (EDL) community. Recently as part of the ESM project, a Lagrangian particle solver named DUst Simulation and Tracking (DUST) [8] has been integrated into the US3D flow code.

The DUST solver provides a time-varying solution for particle attributes such as location, velocity, temperature, and diameter using the Lagrangian-based point-particle discrete element method. Inter-phase and intra-phase interactions, characterized as one, two, or four way coupling between carrier and dispersed phase, can be modeled to varying levels of completeness based on problem requirements within the same framework. A central component of this solver is the particle mesh-location algorithm which utilizes standard unstructured mesh connectivity information to efficiently identify the sequence of Eulerian cells a particle traverses through during the simulation. This also streamlines subsequent operations related to enforcing boundary conditions, parallelization over a distributed memory system, and determining the coupling source terms for the surrounding flow. The time-driven hard-sphere approach is adopted to speed up calculations for resolving particle-particle collisions. Time-stepping is performed using Adams-Bashforth methods which balances temporal accuracy and computational costs.

The US3D-DUST code has been applied to study a range of problems including verification tests involving hypersonic planetary entry, flow through a converging-diverging nozzle, and the impingement of dust particles on a flat plate [8]. Additionally, surface heat-flux augmentation due to particle impacts has been numerically investigated for the Mars 2020 spacecraft during its descent through the dusty Martian atmosphere.

V. Martian Dust Environments

The final preliminary step before running the dust erosion analysis is to estimate what the dust environment will be during entry. The key components to define are the size distribution of the particles and the particle number density as a function of altitude. A commonly used equation to represent atmospheric particle size distribution is the four-parameter modified gamma distribution (MGD) [22]. Based on analysis of the Mariner 9 spectrometer data taken during the 1971 dust storm, Toon, et al. [23] recommended the following form of the MGD for defining the particle size distribution in the Martian atmosphere.

$$N(r) = N_0 r^2 exp\left(-4\left({}^{r}/_{r_m}\right)^{0.5}\right) \tag{28}$$

The modal value of the particle radius, r_m, defines the shape and peak value of the particle distribution. Decreasing the mode radius value compresses the curve to the left, increasing the number of smaller radius particles. Earlier studies such as Toon, et al. [23] and Papadopoulos, et al. [12] used a value of 0.4 micron for the mode radius. Tomasko, et al. [24] suggest a value of 0.32 micron. However, more recent observations by the Mars Climate Sounder (MCS) [25] can be used to estimate a more precise

value of mode radius based on atmospheric conditions on Mars. Profiles of the distribution function based on mode radii of 0.32, 0.35, and 0.40 microns are shown in Fig. 3.

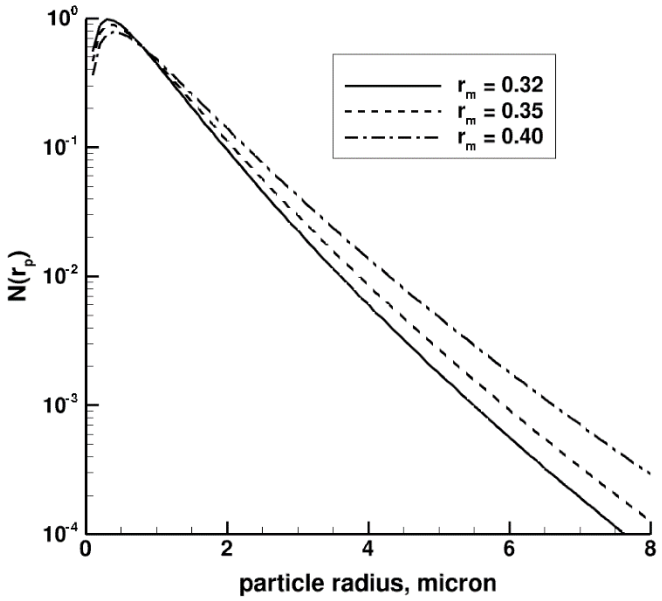


Fig. 3. Number density distribution function as a function of mode radius.

The form of the MCD shown in Eq. (28) represents a number density distribution function. The total particle number density, N_v, is found by integrating the number density distribution function over all particle radii.

$$N_v = \int_0^\infty N(r)\, dr \tag{29}$$

The formal definition of the term $N(r)dr$ is that it represents the number of particles per unit volume with radii between r and $r + dr$. One obstacle in using Eq. (29) to compute total number density is that it requires the value of the N_0 parameter in the $N(r)$ equation, which is not typically known (but can be computed if the total number density is known, i.e., a chicken and the egg situation). In practice, the total particle number density can be determined from atmospheric and dust environment conditions, which is described later in this section, and then N_0 could be determined from that value if desired.

A normalized distribution function, $n(r)$, can be defined where the number density distribution function for any radius, r, is divided by the total particle number density.

$$n(r) = \frac{1}{N_v} N(r) = \frac{N(r)}{\int N(r) dr} \tag{30}$$

One advantage of using the normalized distribution function is it can be evaluated without having to know the value of the N_0 parameter, since it appears in both the numerator and denominator. The integral of the normalized distribution function over all particle radii is equal to 1. One of the properties of the normalized distribution function is that the average value of a function, $F(r)$, for all particles in the distribution is found by integrating the product of $F(r)$ and the normalized distribution function over all particle radii.

$$F_{avg} = \int_0^\infty F(r)n(r)\,dr \tag{31}$$

Because of this feature, the normalized distribution function can be used to compute the average spherical particle cross-sectional area or volume in Martian dust environment, which are useful when computing the particle number density from opacity values measured in the Martian atmosphere.

As mentioned in a previous paragraph, MCS data can be used to estimate the mode radius and the particle number density in the Martian atmosphere. The MCS is one component of Mars Reconnaissance Orbiter (MRO) spacecraft that has been making global, moderate vertical resolution observations of infrared radiance from Mars's limb, nadir, and off nadir in nine broadband channels sensitive to dust, temperature, and other aerosols since 2006 [25]. Atmospheric retrievals from MCS observations include vertical profiles of temperature and dust opacity, i.e., fractional extinction due to dust per unit height, $d_z\tau$, at 463 cm−1 (the center of MCS's A5 channel). The MCS retrieval algorithm was based on the dust being compositionally uniform and made of spherically symmetric particles with a modified gamma size distribution shown in Eq. (28).

To be precise, the MCS measures the density-scaled opacity, which is simply the dust opacity divided by the atmospheric density. The density at a given altitude can be obtained from the Best Estimated Trajectory (BET) data, and the dust opacity can be determined using that value. The dust opacity can be related to the total number density of dust particles, N_v.

$$d_z\tau = Q_{ext}N_vG \tag{32}$$

Dust opacity is typically expressed in units of 1/km. To compute particle number density, this quantity needs to be computed to 1/m. The quantity, G, in Eq. (32) is the average cross-sectional area of the particles over the entire distribution. For spherical particles, the average cross-sectional area can be determined from Eq. (31) using $F(r) = \pi r^2$. The quantity, Q_{ext}, is a dimensionless constant known as the extinction coefficient. The MSC retrieval algorithm set its value to be 0.35 [25], but its value has been shown to be a function of the effective particle radius, which is proportional to the average particle volume divided by the average cross-sectional area.

In this paper, the particle drag models and subsequent heatshield erosion were evaluated during a major global dust storm in the Martian atmosphere, certainly the worst-case scenario for spacecraft designers. The conditions selected were those measured during the 2007 major global dust storm. The mode radius for the distribution function was set to 0.41 microns, which corresponds to an effective radius of 3 microns – a typical value estimated to occur during a dust storm. The extinction coefficient under these conditions was 1.24.

Profiles of measured dust opacity and estimated particle number density during the 2007 major global dust storm are shown in Fig. 4. Also shown in the figures are profiles during quiescent dust conditions measured by the MCS in 2012. As would be expected, during the global dust storm significant dust levels were seen at much higher altitudes and the particle number densities were orders of magnitude higher at an equivalent altitude compared to quiescent dust conditions.

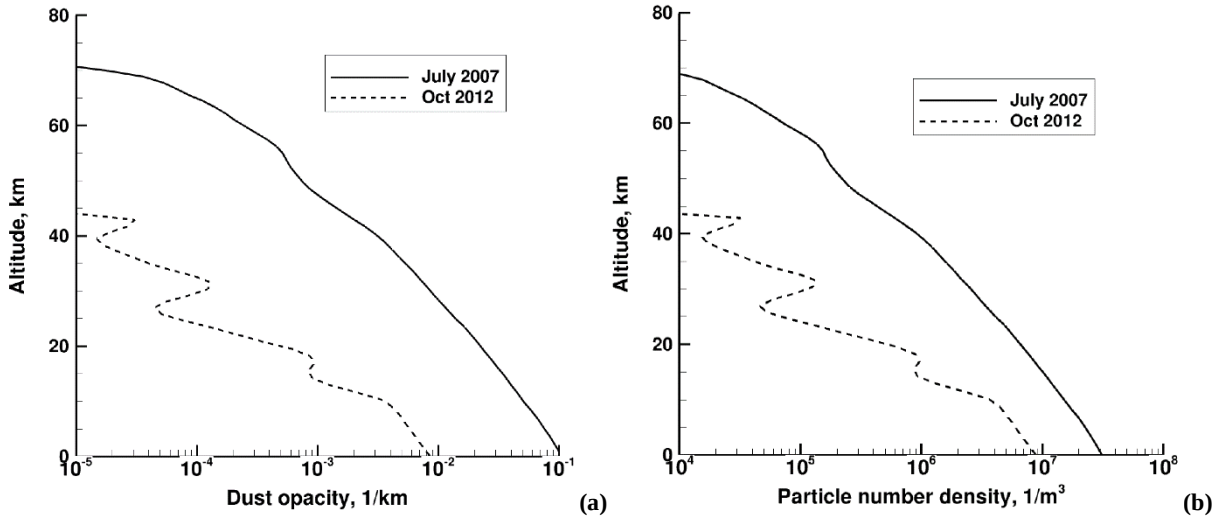


Fig. 4. Dust environments during the 2007 global dust storm. (a) dust opacity. (b) particle number density.

VI. Heatshield Recession due to Dust Particle Impacts

As reported in more detail in Ref. [1], A dust particle striking the heatshield with sufficient kinetic energy will cause spallation damage to the TPS material. In addition to particle kinetic energy, the composition, density, and strength of both the particle and the heatshield are factors in how much damage a particle impact will cause. Previous work on impact cratering by Greely and Schulz [26] determined that the crater diameter is approximately proportional to the cube root of the particle kinetic energy. This scaling relationship was found to be approximately valid over orders of magnitude of both energy and particle size, and several of the surface damage correlations presented in this section are based on this scaling. For spherical particles of uniform composition, the kinetic energy can be expressed in terms of the particle density, diameter, and velocity.

$$K.E. = \frac{\pi}{12}\rho_p d_p^3 V_p^2 \tag{25}$$

Using the cube root relationship to kinetic energy, the crater diameter for a particle impact would take the general form shown in Eq. (26).

$$D_c = C\rho_p^{1/3} d_p {v_p}^{2/3} \tag{26}$$

The value of the leading coefficient, C, would be a function of both the particle and the material it impacted. In general, impact crater damage correlations for a specific TPS material do not follow the idealized form shown in Eq. (26). Updated values for the exponents on the particle density, diameter, and impact velocity are obtained from experiments. There were a number of damage correlation experiments performed in the 1960's and 70's in support the Apollo and Space Shuttle programs for materials such as AVCOAT [27] and LI-900 and LI-2200 Space Shuttle tiles [28].

The TPS material used in this paper to evaluate the effect of particle drag model on surface recession is Norcoat Liège [29] that was used on the heatshield of the Schiaparelli entry capsule [30]. Norcoat Liège is a charring, ablative material made from cork particles infused with a phenolic resin. It has a material density of 470 kg/m^3.

A series of hot erosion tests were performed in the German Aerospace Center (DLR) L2K arcjet facility to assess the surface erosion due to dust particle impacts in Norcoat Liège [29]. The test articles

were 0.1m diameter, flat, circular disks of Norcoat Liège. The models were exposed to heating rates ranging from 15-45 W/cm^2 for test times of 90 and 145 seconds. The L2K test facility had the ability to inject particles made from boron nitride (BN) and Al_2O_3 into the flow to measure material erosion due to dust particle impacts. Particle diameters used in the experiments ranged from 0.5 to 15 microns, which is consistent with the size of Martian dust particles. The models were weighed before and after the test to determine the total mass lost during the test time

Using experimental particle erosion data taken in the DLR L2K arcjet facility, Palmer, et al. [1] derived an expression for the impact crater diameter caused by a particle impact into Norcoat Liège. Several assumptions were made in deriving the damage correlation. The crater shape was assumed to be hemispherical, and the total mass loss due to particle impacts measured during the test is assumed to be equal to the sum of the individual particle impacts. Using these assumptions, impact crater diameter can be expressed in the form shown in Eq. (26) as a function of the particle diameter, particle density, and impact velocity.

$$D_c = 0.00056\rho_p^{0.62} d_p^{1.04867} v_p^{0.667} \tag{27}$$

Since the craters were assumed to be hemispherical, the crater depth would be simply one half the diameter. As developed by Papadopoulos, et al. [12], the cumulative heatshield recession caused by dust particle impacts is a function of the crater diameter, crater depth, average impact angle, and the total number of particles, N_p, that strike the heatshield per unit area. The Norcoat Liège surface damage correlation shown in Eq. (27) has been incorporated into the US3D-DUST code.

Looking at Eq. (27), the size of the particle impact crater is a function of both the particle diameter and the impact velocity. Smaller particles will be more affected by aerodynamic drag force as they travel through the shock layer. This effect is shown in Figure 5a, taken from Ref. [1], that shows computed particle impact velocity at the stagnation point at flow conditions corresponding to the the Schiaparelli 35 km trajectory point. These results were based on the Henderson drag model. While the smaller particles decelerate more rapidly and do less damage per impact, there are more of them. The combination of particle size, impact velocity, and number density defines the surface recession rate. Figure 5b, also taken from Ref. [1], shows the recession rate as a function of particle size along the Schiaparelli entry trajectory. The largest contributors to surface recession are particles with diameters between the 3- and 6-microns. The 1- and 2-micron particles, while there are more of them, decelerate sufficiently in the shock layer such that they don't contribute as much to the overall surface recession rate.

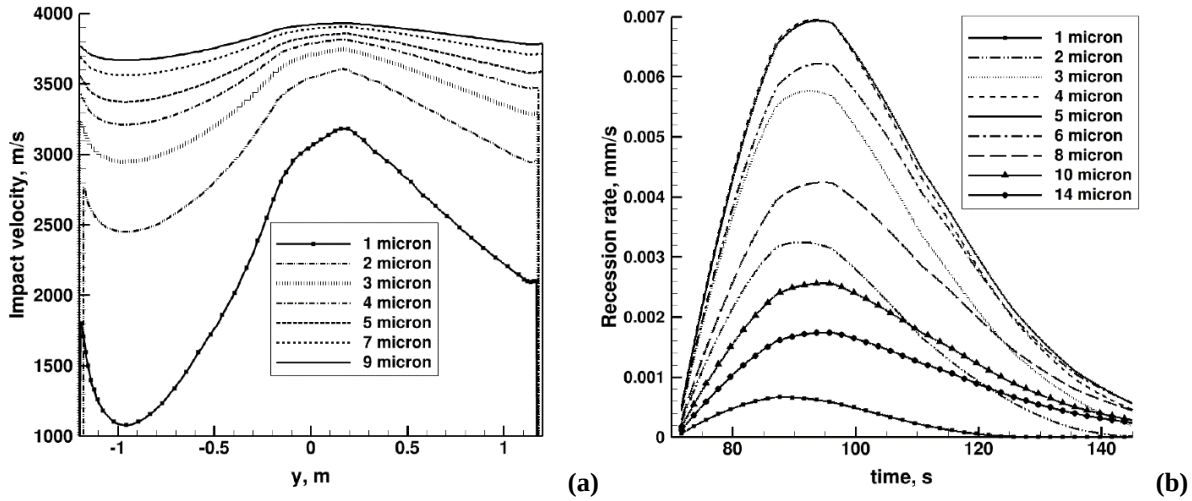


Fig. 5. Particle trajectory results for 2007 global dust storm conditions as a function of particle diameter. (a) impact velocity (b) rate of surface recession due to dust particle impacts.

VII. Results

A. Martian shock layer environments

The Henderson and Loth drag models described and evaluated in this paper are designed to cover a wide range of flow conditions including Reynolds numbers up to 2.0×10^5 and Knudsen numbers ranging from continuum to free-molecular flow values. The focus for the drag model comparisons in this paper is to determine the effect on heatshield erosion due to dust particle impacts on a spacecraft entering the atmosphere of Mars during a dust storm. In addition to the Henderson and Loth particle drag models, the simpler Clift-Gauvin particle drag model that is intended for incompressible, continuum particle flow conditions will be analyzed to assess the impact rarefaction and compressibility effects have inside Martian shock layers.

When assessing particle drag models for Martian entry applications, it is important to identify the flow regimes that particles will experience when traveling through a Martian shock layer. As part of a dusty-flow analysis in the Martian atmosphere, Palmer, et al. [1] generated a series of CFD solutions over the Schiaparelli entry capsule [30]-[31]. The freestream conditions for the seven trajectory points used in this study are shown in Table 3. They range from 20.9 to 50 km in altitude and represent the range where noticeable surface recession due to dust particle impacts is expected.

Table 3. Schiaparelli CFD trajectory points.

Time, s	Altitude, km	Density, kg/m^3	Velocity, m/s	Temperature, K	Angle of attack, deg
71.7	50.0	1.755e-4	5500.6	171.8	7.2
78.9	45.0	2.944e-4	5185.0	175.0	7.2
87.2	40.0	4.825e-4	4689.0	182.4	7.2
96.3	35.0	7.717e-4	4016.9	186.3	7.2
110.8	30.0	1.322e-3	2913.7	190.1	6.0
125.6	25.5	1.979e-3	2013.8	195.4	5.0
145.6	20.9	2.962e-3	1236.9	202.3	3.0

In order to determine the particle flow environments inside the shock layer around the Schiaparelli capsule, the US3D-DUST code was used to simulate the trajectories of 2-micron and 10-micron diameter particles traveling through the shock layer at the trajectory points at altitudes between 25.5 and 40 km. These trajectory points were chosen because analysis performed in Ref. [1] indicated that this altitude range is where most of the heatshield erosion due to dust particle impact damage will occur. The particle sizes of 2- and 10-microns bound the range of particle diameters that will contribute to heatshield recession. The particles were assumed to be spherical with a material density of 2940 kg/m^3, which is an value for the material density of Martian dust particles estimated by Papadopolous, et al. [12].

The dust environments in the Martian shock layer predicted by US3D-DUST are shown in Fig. 5. The Loth particle drag model was used in these simulations. Because the shock standoff distance is different for each case, the value along the x-axis is the normalized distance from the wall to the shock, with the value of -1 representing the shock location. As shown in Fig. 5a, the particle Reynolds number values vary from about 0.4 to 6 in the shock layer, with the larger 10-micron particles having higher Reynolds number values. Based on these shock layer simulations, Martian dust particles are in the rarefaction-dominated regime.

The particle Mach numbers, shown in Fig. 5b, exhibit a relatively narrow range with values between 2 and 4, indicating the particles are in the compressible, supersonic flow regime. Knudsen number profiles, shown in Fig. 5c, vary from about 0.8 to 10, indicating that the dust particles are in the transitional flow regime.

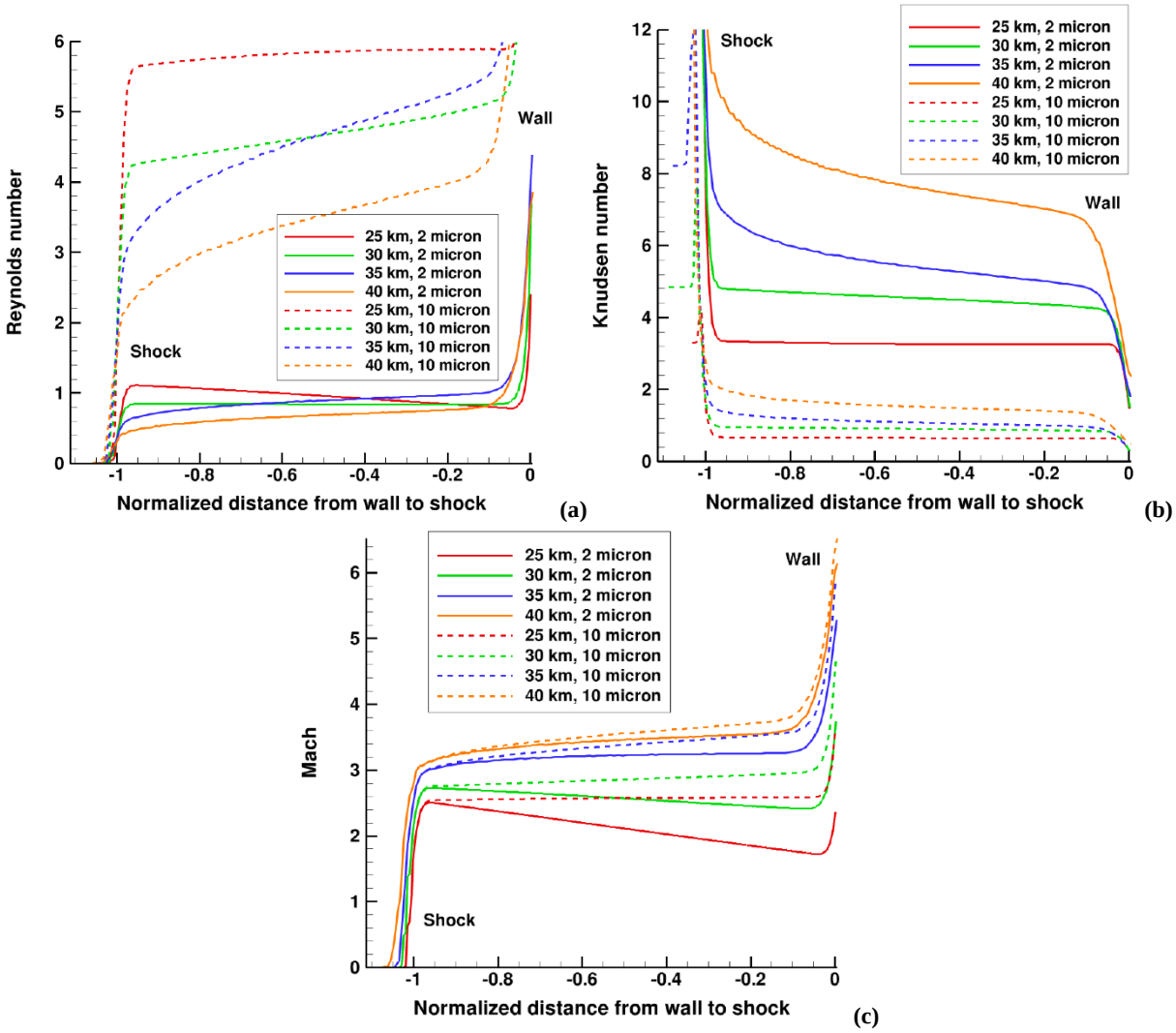


Figure 5. Particle flow characteristics in Martian shock layers. (a) Reynolds number (b) Mach number (c) Knudsen number.

The ranges for the particle Reynolds, Mach, and Knudsen numbers in the Schiaparelli shock layers and the corresponding flow regimes are summarized in Table 4. Martian dust particles will not be in the continuum flow regime due to their small size (generally less than 10-micron in diameter) and the low density of the Martian atmosphere, both of which contribute to small particle Reynolds numbers. Continuum flow requires large Reynolds numbers and/or Mach numbers much less than 1.

Table 4. Summary of particle flow conditions in Martian shock layer.

Quantity	Range	Regime
Re	0.4 – 6	Rarefaction-dominated

Mach	2 – 4	Compressible, supersonic
Kn	0.8 – 10	Transitional

B. Particle velocity and drag coefficient profiles

While it is not covered in detail in this paper, the shock layer temperatures during the Schiaparelli entry are not high enough to cause sublimation of the dust particles [1], so the particle diameter will be constant during the particle trajectory. The heatshield recession will therefore be driven by the impact velocity of the particles, which will be determined by the choice of particle drag model. Particle trajectories were computed for 2-, 4-, 5-, and 8-micron diameter dust particles as they traveled through the shock layer along the stagnation line at the 35 km altitude trajectory point. Velocity profiles in the shock layer are shown in Fig. 6. Note that the y-axis ranges are different in the plots to highlight the differences between the drag methods.

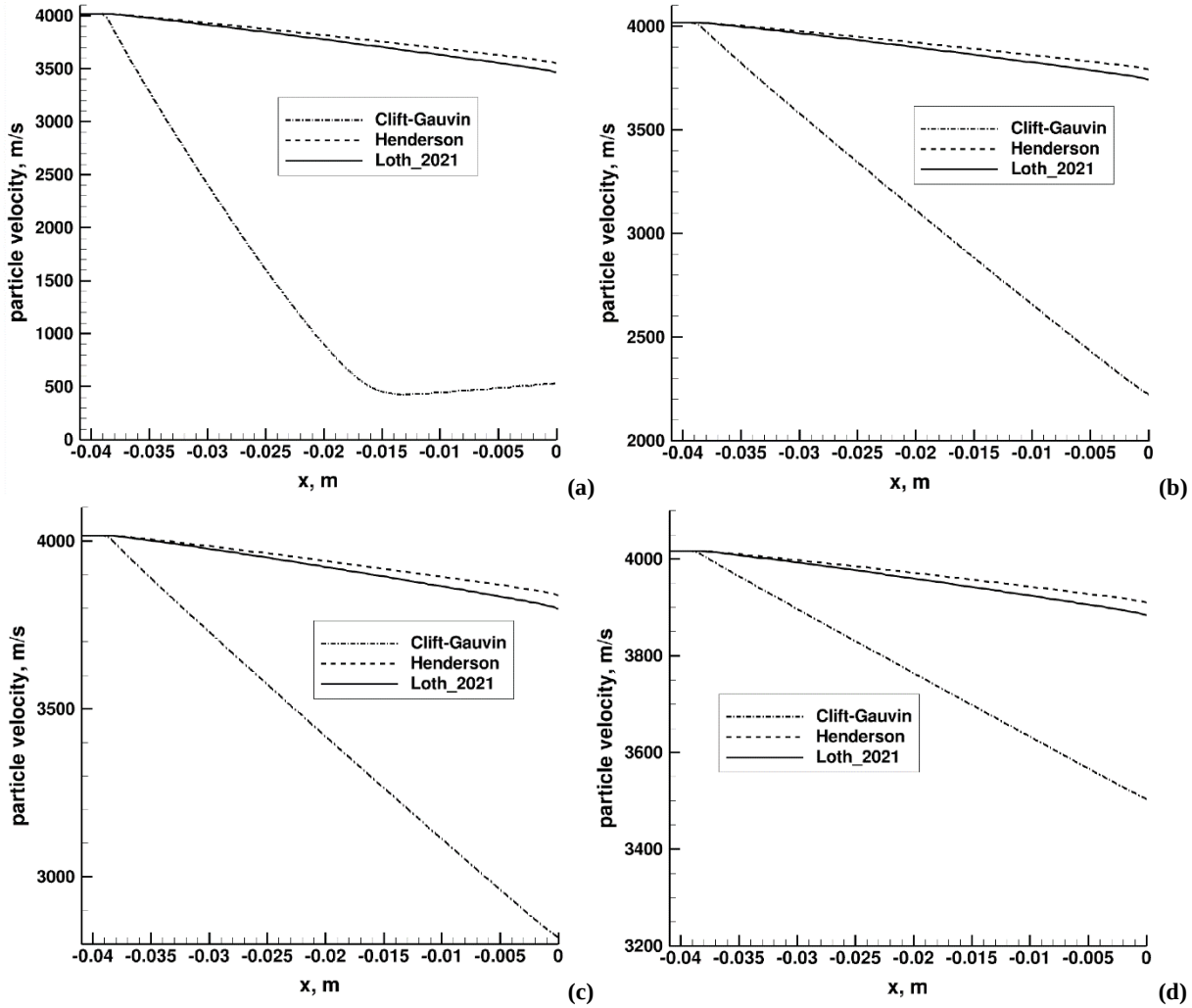


Fig. 6. Velocity profiles of particles traveling through the 35 km altitude shock layer. (a) 2-micron (b) 4-micron (c) 5-micron (d) 8-micron

It is evident from the velocity profiles shown in Fig. 6 is that there is a large difference in predicted particle velocity using the Clift-Gauvin drag model compared to the profiles using the Henderson or Loth models. The difference in particle velocity is greatest for the smallest, 2-micron particles, because smaller particles are more affected by aerodynamic drag forces. The Clift-Gauvin model is intended for incompressible, continuum particle flow conditions whereas particles traveling through a Martian shock layer will experience compressible, transitional flow. The velocity profiles indicate that neglecting Knudsen number and compressibility effects in the rarefaction-dominated drag regime over-predicts the particle drag coefficient and the deceleration of the particle as it travels through the shock layer.

There is a reasonably close correlation between the Henderson and Loth drag model velocity profiles. The velocities using the Loth drag model are lower than the Henderson profiles implying that the Loth-2021 drag model predicts slightly lower particle drag coefficients. This implication is confirmed in Fig. 7 where drag coefficient profiles through the 35-km altitude trajectory point are displayed for the 2- and 5-micron diameter particles. The Loth drag coefficient values are higher by a small, nearly constant amount compared to the Henderson values. In contrast, the drag coefficients computed using the Clift-Gauvin drag model are one or more orders of magnitude higher compared to the Loth or Henderson values.

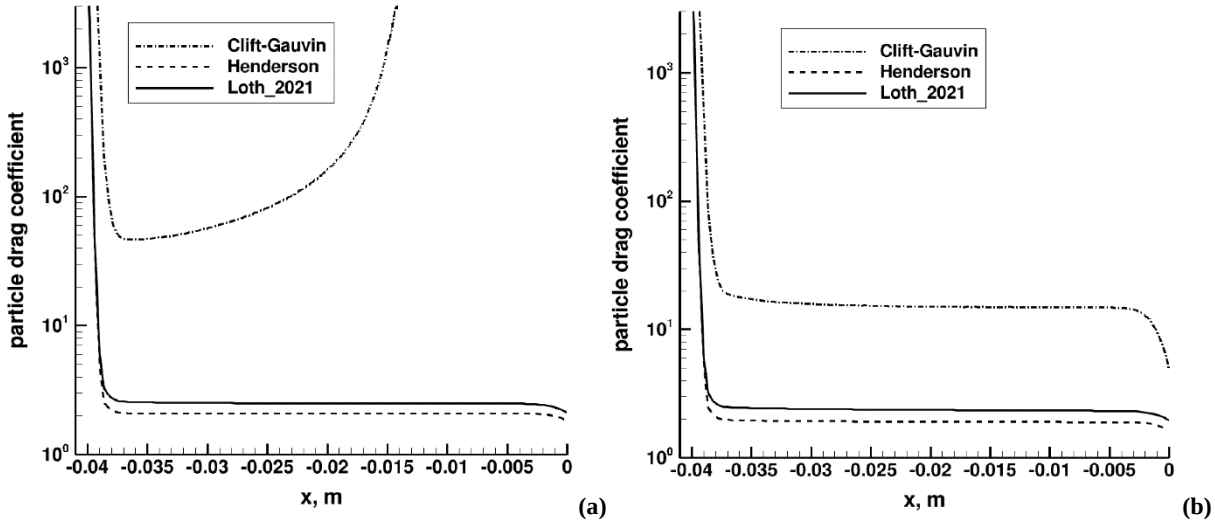


Fig. 7. Drag coefficient profiles of particles traveling through the 35km altitude shock layer. (a) 2-micron diameter particles. (b) 5-micron diameter particles.

To assess the effect of drag model on particle drag coefficient and velocity as a function of altitude, trajectories for 4-micron diameter particles were computed along the stagnation line at the seven Schiaparelli trajectory points. The values along the x-axis in the plots are the normalized distances from the shock to the wall, with a value of -1 representing the shock location. Figure 8a shows particle drag coefficient. As was the case with the results seen in Fig. 7, the Loth drag model predicts higher drag coefficients compared to the Henderson model at every trajectory point. An interesting element of Fig. 8a, is that the Henderson curve at the 21 km trajectory point shows a linear behavior near the wall that is due to the gap in the Henderson drag model between particle Mach numbers of 1.0 and 1.75. The Loth drag model shows a greater spread in drag coefficient values as a function of altitude compared to the Henderson profiles, and the spread in the Loth values increases as the particle approaches the wall.

The velocity profiles as a function of altitude are shown in Fig. 8b. Despite the significant differences in drag coefficients predicted by the Loth and Henderson drag models shown in Fig. 8a, the velocity profiles in Fig. 8b are similar between the Henderson and Loth drag models with the Loth drag model predicting slightly lower particle velocities throughout the shock layer at all seven trajectory points. In

part, the similarity between the Henderson and Loth velocity profiles is due to the rapid transit time of the 4-micron diameter particles through the shock layer. Even at the 21 km trajectory point, which has the thickest shock layer, the 4-micron particles only take 0.16 milliseconds to travel through the shock layer. Therefore, the transit time is too short for the difference in drag coefficients to have much effect on the velocity profiles.

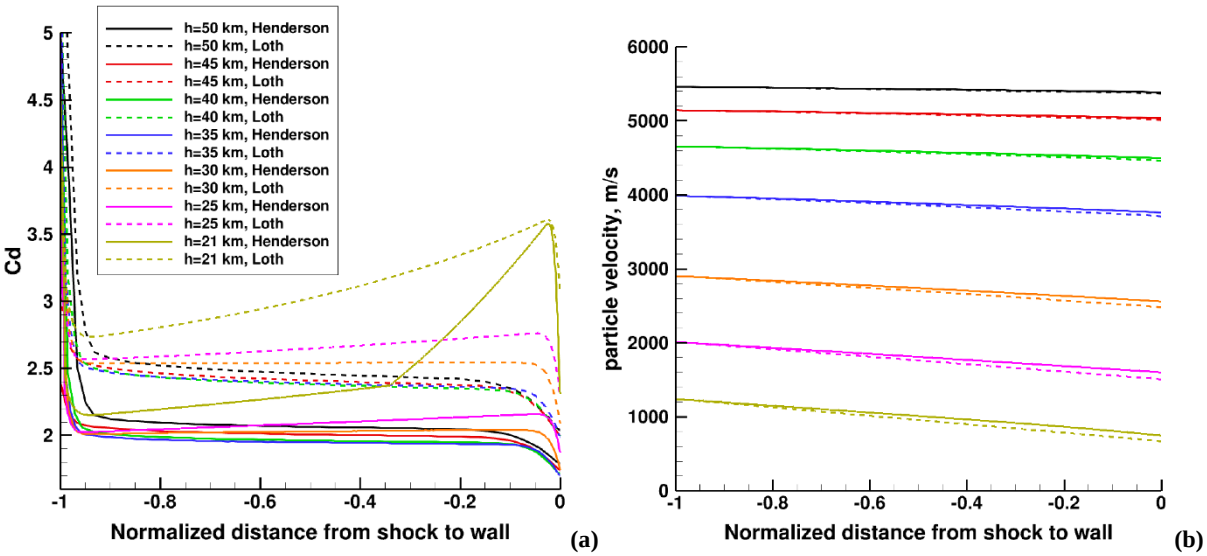


Fig. 8. Shock layer profiles for 4-micron particles at different Schiaparelli trajectory points. (a) drag coefficient. (b) particle velocity.

C. Effect of drag model on surface recession rates

To assess the effect of particle drag model on the heatshield recession due to dust particle impacts, the US3D-DUST code was used to compute dusty flow conditions at the seven Schiaparelli trajectory points. The particles were assumed to be spherical with a material density of 2940 kg/m^3. The initial particle velocities were set to be equal to the freestream flow values shown in Table 3. While the details were not covered in this paper, one-way fluid-particle coupling was assumed where the surrounding fluid affected the particles, but the particles had no effect on the surrounding fluid. The particle distribution was set using the MGD function shown in Eq. (28) as well as measured MCS data from the 2007 major global dust storm.

US3D-DUST uses a random number generation to seed particles on the faces of the outer boundary of the CFD grid according to the particle size distribution. The code solves the coupled ODE's that characterize the particle trajectories until either the particles strike the surface or leave the computational domain. The US3D-DUST code uses the surface damage correlation for Norcoat Liège shown in Eq. (27) to compute the size of the impact crater when a dust particle strikes the surface, and the code is able to combine the contributions of all the particle impacts to compute the average recession rate and each surface grid face. Integrating the recession rate over the entire trajectory space allows an estimate of the total surface recession on the heatshield due to particle impacts.

The predicted recession rate at the stagnation point for the seven Schiaparelli trajectory points is shown in Fig. 9a. Due to the way particles are seeded at the outer boundary of the CFD grid, there is some noise in the average recession rate computed by US3D-DUST at every surface grid face. To smooth out this noise, the values shown in Fig. 9a are averages taken over a small surface grid domain surrounding

the stagnation point. Also shown in Fig. 9a is the recession rate of is Norcoat Liège due to thermochemical ablation predicted by the Icarus material response code [34]. As would be expected from the particle velocity profiles shown in Fig. 8b, the particle impact recession rates computed by the Henderson and Loth drag models are similar with the Henderson model predicting slightly higher recession rates along the entire trajectory space. The cumulative surface recession over the seven trajectory points is shown in Fig. 8b. The total surface recession predicted using the Henderson drag model was 2.11 mm compared to 2.01 mm if the Loth particle drag model is used. This difference is well within the uncertainty of the overall particle impact solution process. The surface recession caused by dust particle impacts is comparable to that caused by thermochemical ablation of Norcoat Liège, which was estimated to be 2.51 mm.

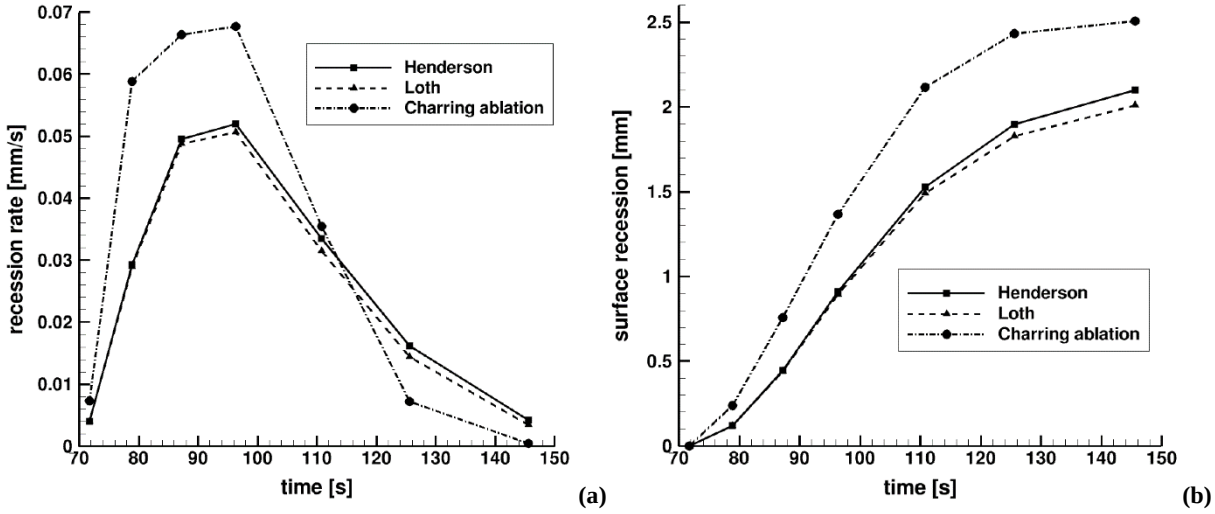


Fig. 9. Effect of particle drag model on surface recession. (a) recession rate. (b) cumulative recession. [ADD CLIFT-GAUVIN TO THESE PLOTS]

VIII.Concluding Remarks

This paper presented an evaluation of the effect particle drag model has on the predicted surface recession due to dust particle impacts on the heatshield of a spacecraft entering the Martian atmosphere during a major global dust storm. The concepts of particle Reynolds, Mach, and Knudsen numbers were presented as a way to characterize particle flow conditions. A brief overview was provided of the solution methodology to characterize the Martian dust environment and how surface damage correlations are derived for particle impacts.

Three particle drag models were evaluated. The Clift-Gauvin drag model is intended for incompressible, continuum particle flow conditions. The Henderson and Loft drag models are intended for a wide range of particle flow conditions. The assumptions, derivations, applicability, and underlying experimental data for each of the drag models was discussed.

The US3D-DUST code was used to compute particle trajectories at seven points along the Schiaparelli capsule Martian entry trajectory. The dust conditions used were based on MCS data taken during the 2007 major global dust storm. Analysis of particle trajectories through the shock layer indicated that the particles would be in the compressible, transitional flow regimes. Particle trajectory profiles through the shock layer indicated that ignoring Knudsen number and compressibility effects (i.e., assuming

incompressible, continuum flow) greatly over-estimated particle drag coefficient and the deceleration of the particles in the shock layer. A drag model that includes Knudsen number and compressibility effects is important for Martian dusty flow analysis.

The Loth drag model predicted higher particle drag coefficients throughout the shock layer at all seven Schiaparelli trajectory points compared to the Henderson model. The gap in the Henderson drag model between Mach numbers of 1.0 and 1.75 was evident at the lowest 21 km trajectory point drag coefficient profile. Due to the short transit time through the shock layer, there was a smaller difference in particle velocity predicted by the two models than was evident in the drag coefficient profiles, with the Henderson model generated slightly higher particle velocities. In terms of recession rate due to particle impacts, the Henderson model predicted slightly higher values compared to the Loth results. The overall heatshield recession at the stagnation point was 2.11 mm for the Henderson model and 2.01 mm for the Loth model, a difference that is well within the uncertainty of the overall particle impact solution process. Both drag models predicted that the heatshield recession due to dust particle impacts during a major global dust storm is comparable to that caused by thermochemical ablation of the Norcoat Liège TPS material

One of the main differences between the Henderson and Loth drag models is the Loth model is based on additional experimental and DSMC data in the slip and transitional flow regimes, which is relevant in Martian shock layers, so presumably the Loth drag model is the more accurate of the two. However, there was not sufficient difference between the two drag models to indicate a clear choice between the two for Martian shock layer analysis. One important conclusion is that the particle drag model must account for Knudsen number and compressibility effects.

One item beyond the scope of this paper is an analysis of the effect of non-spherical particles on heatshield recession due to dust particle impacts. Haider and Levenspiel [32] developed a particle drag model for incompressible, continuum flow that included the effects of sphericity that matched experimental data on the terminal velocity of non-spherical particles dropped from a height. They found that the drag coefficient increased with decreasing sphericity (a perfect sphere has a sphericity value of 1). Allofs, et al. saw a similar result in experiments performed in the DLR GBK facility [33] where a larger value of drag coefficient than that predicted by the spherical drag models was required to match experimental data of particle velocity at the GBK nozzle exit.

When applied to Martian shock layers, accounting for non-spherical particles effects will increase the particle drag coefficient, decrease the impact velocity, and decrease the amount of heatshield recession due to particle impacts. Therefore, using the spherical drag models described in this paper is a conservative approach in the analysis of heatshield recession due to particle impacts.

References

[1] Palmer, G., Ching, E., Ihme, M., Allofs, D., and Gülhan, A., "Modeling Heatshield Erosion due to Dust Particle Impacts for Martian Entries," *Journal of Spacecraft and Rockets*, Vol. 57, No. 5, 2020, pp. 857-875.

[2] Loth, E., "Supersonic and Hypersonic Drag Coefficients for a Sphere", *AIAA Journal*, Vol. 59, No. 8, 2021, pp. 3261-3274.

[3] Loth, E., "Compressibility and Rarefaction Effects on Drag of a Spherical Particle", *AIAA Journal*, Vol. 46, No. 9, 2008, pp. 2219-2228.

[4] Stokes, G. G., "On the Effect of the Internal Friction of Fluids on the Motion Of Pendulums," Transactions of the Cambridge Philosophical Society (Mathematical and Physical Sciences), Vol. 9, Pt. 2, 1851, pp. 8–106.

[5] Henderson, C.B., "Drag Coefficients of Spheres in Continuum and Rarefield Flows," *AIAA Journal*, Vol. 14, No. 6, 1976, pp. 707-718.

[6] Clift, R., and Gauvin, W. H., Proceedings of CHEMECA ’70, Vol. 1, Butterworth, Melbourne, 1970, pp. 14–28.
[7] Schiller, L., and Naumann, A. Z., “Über die Grundlegenden Berechungen bei der Schwerkraftaufbereitung,” Zeitschrift des Vereines Deutscher Ingenieure, Vol. 77, No. 12, 1933, pp. 318–320.
[8] Sahai, A. and Palmer, G. “A Variable Fidelity Euler-Lagrange Framework for Simulating Particle-Laden High-Speed Flows,” *AIAA Journal*, Vol. 60, No. 1, October 2022.
[9] Gülhan, A., Thiele, T., Siebe, F., Kronen, R., and Schleutker, T., “Aerothermal Measurements from the ExoMars Schiaparelli Capsule Entry,” *J. of Spacecraft and Rockets*, Vol. 56, No. 1, 2019, pp. 68-81.
[10] Allofs, D., Neeb, D., and Guelhan, A., “Simultaneous determination of particle size, velocity, and mass flow in dust-laden supersonic flows,” Experiments in Fluids (2022), 63:86, https://doi.org/10.1007/s00348-022-03402-z.
[11] Bailey, A.B. and Hiatt, J., “Free-Flight Measurements of Sphere Drag at Subsonic, Transonic, Supersonic, and Hypersonic Speeds for Continuum, Transition, and Near-Free-Molecular Flow Conditions,” AEDC-TR-70-291, 1971.
[12] Papadopoulos, P., Tauber, M., and Chang, I-D., “Heat Shield Erosion in a Dusty Martian Atmosphere”, *Journal of Spacecraft and Rockets*, Vol. 30, No. 2, 1993, pp. 140-151
[13] Millikan, R. A., "Coefficients of Slip in Gases and the Law of Reflection of Molecules From the Surfaces of Solids and Liquids,"*Physical Reviews,* Vol. 21, March 1923, pp. 217-238.
[14] Millikan, R. A., "The General Law of Fall of a Small Spherical Body Through a Gas, and Its Bearing Upon the Nature of Molecular Reflection From Surfaces," *Physical Reviews*, Vol. 22, July 1923, pp. 1-23.
[15] Hoerner, S. F., Fluid-Dynamic Drag, published by Hoerner, S. F., Midland Park, NJ, 1958.
[16] Carlson, D. J., and Hoglund, R. F., “Particle Drag and Heat Transfer in Rocket Nozzles,” AIAA Journal, Vol. 2, No. 5, 1964, pp. 1980–1984.
[17] Macrossan, M. N., “Scaling Parameters in Rarefied Flow and the Breakdown of the Navier-Stokes Equations,” Department of Mechanical Engineering, University of Queensland, Tech. Rept. 2004/09, 2004.
[18] Clift, R., and Gauvin,W. H., “The Motion of Entrained Particles in Gas Streams,” Canadian Journal of Chemical Engineering, Vol. 49, No. 4, Aug. 1971, pp. 439–448.
[19] Stadler, J. R., and Zurick, V. J., “Theoretical Aerodynamic Characteristics of Bodies in Free-Molecule Flow Field,” NACA TN 2423, 1951, p. 12.
[20] Schaaf, S. A., and Chambré, P. L., “The Flow of Rarefied Gases,”Section of Fundamentals of Gas Dynamics, edited by H. W. Emmons, Princeton Univ. Press, Princeton, NJ, 1958.
[21] Candler, G.V., Johnson, H.B., Nompelis, I., Gidzak, V.M., Subbareddy, P.K., and Barnhardt, M., “Development of the US3D code for advanced compressible and reacting flow simulations,” AIAA Paper 2015-1893, Jan. 2015.
[22] Petty, G.W. and Huang, W., “The Modified Gamma Size Distribution Applied to Inhomogeneous and Nonspherical Particles: Key Relationships and Conversions,” J. of the Atmospheric Sciences, Vol. 68, 2011, pp. 1460 – 1473.
[23] Toon, O.B., Pollack, J.B., and Sagan, C., “Physical Properties of the Particles Composing the Martian Dust Storm of 1971-1972,” *Icarus*, Vol. 30, 1977, pp. 663-696.
[24] Tomasko, M.G., Doose, I.R., Lemmon, M., Smith, P.H., and Wegryn, E., “Properties of dust in the Martian atmosphere from the Imager on Mars Pathfinder,” *J. of Geophys. Research*, Vol. 104, No. E4, 1999, pp. 8987-9007.

[25] Heavens, N.G., et al., “The vertical distribution of dust in the Martian atmosphere during northern spring and summer: Observations by the Mars Climate Sounder and analysis of zonal average vertical dust profiles,” *Journal of Geophysical Research*, Vol. 116, 2011.
[26] Greely, R. and Schultz, P. ed., A Primer in Lunar Geology, Gault, D., "Impact Cratering," NASA TM-62,359, July 1974.
[27] Cour-Palais, B.G., “Hypervelocity Impact Investigations and Meteoroid Shielding Experience Related to Apollo and Skylab,” *Proceedings of the Orbital Debris Workshop*, edited by D. Kessler and S-Y. Su, NASA Conference Publication 2360, 1985.
[28] Christiansen, E.L. and Ortega, J.,"Hypervelocity Impact Testing of Shuttle Orbiter Thermal Protection System Tiles," AIAA Paper 90-3666, Sept. 1990.
[29] Keller, K., Lindenmaier, P., Pfeiffer, E.K., Esser, B., Gülhan, A., Marraffa, L., Omaly, P., and Desjean, M.C., “Dust Particle Erosion during Mars Entry,” AIAA Paper 2010-6283, 2010.
[30] Gülhan, A., Thiele, T., Siebe, F., Kronen, R., and Schleutker, T., “Aerothermal Measurements from the ExoMars Schiaparelli Capsule Entry,” *J. of Spacecraft and Rockets*, Vol. 56, No. 1, 2019, pp. 68-81.
[31] Johnstone, E., Stindt, T., Merrifield, J., and Ferracina, L., “Analysis of the Aerothermal and Material Performance During the ExoMars Schiaparelli Descent,” *International Conference on Flight Vehicles, Aerothermodynamics, and Re-entry Missions & Engineering* (FAR), 2019.
[32] Haider, A.M., and Levenspiel, O., “Drag coefficient and terminal velocity of spherical and nonspherical particles,” *Powder Technology*, 58-1, 1989, pp. 63 – 70.
[33] Allofs, D., Neeb, D., and Guelhan, A., “Simultaneous determination of particle size, velocity, and mass flow in dust-laden supersonic flows,” Experiments in Fluids (2022), 63:86, https://doi.org/10.1007/ s00348-022-03402-z.
[34] Schulz, J.C., Stern, E.C., Muppidi, S., and Palmer, G.E., “Development of a Three-Dimensional, Unstructured Material Response Design Tool,” AIAA Paper 2017-0667, 2017.

[14] https://atmos.nmsu.edu/data_and_services/atmospheres_data/MARS/mcs.html